Paleoceanography and Paleoclimatology

RESEARCH ARTICLE
10.1029/2021PA004221

Key Points:

- We present sub-centennial temperature and salinity records from the Gulf of Mexico (GoM) using paired foraminiferal δ^{18}O-Mg/Ca geochemistry
- We uncover large (~2°C) millennial-scale temperature swings and document a salinification trend since the early-to-mid Holocene
- Synthesis of GoM-wide paleoceanographic surface-ocean records suggests a dynamic and variable Holocene history

Supporting Information:

Supporting Information may be found in the online version of this article.

Correspondence to:

K. Thirumalai,
kaustubh@arizona.edu

Citation:

Thirumalai, K., Richey, J. N., & Quinn, T. M. (2021). Holocene evolution of sea-surface temperature and salinity in the Gulf of Mexico. *Paleoceanography and Paleoclimatology*, *36*, e2021PA004221. https://doi.org/10.1029/2021PA004221

Received 19 JAN 2021
Accepted 26 JUL 2021

Holocene Evolution of Sea-Surface Temperature and Salinity in the Gulf of Mexico

Kaustubh Thirumalai[1], Julie N. Richey[2], and Terrence M. Quinn[3,4]

[1]Department of Geosciences, University of Arizona, Tucson, AZ, USA, [2]U.S. Geological Survey, St. Petersburg Coastal and Marine Science Center, St. Petersburg, FL, USA, [3]Institute for Geophysics, University of Texas at Austin, Austin, TX, USA, [4]Department of Geological Sciences, Jackson School of Geosciences, University of Texas at Austin, Austin, TX, USA

Abstract Flows into and out of the Gulf of Mexico (GoM) are integral to North Atlantic Ocean circulation and help facilitate poleward heat transport in the Western Hemisphere. The GoM also serves as a key source of moisture for most of North America. Modern patterns of sea-surface temperature (SST) and salinity in the GoM are influenced by the Loop Current, its eddy-shedding dynamics, and the ensuing interplay with coastal processes. Here, we present sub-centennial-scale records of SST and stable oxygen isotope composition of seawater ($\delta^{18}O_{sw}$; a proxy for salinity) over the past 11,700 years using planktic foraminiferal geochemistry in sediments from the Garrison Basin, northwestern GoM. We measured δ^{18}O and magnesium-to-calcium ratios in tests of *Globigerinoides ruber* (white) to generate quantitative estimates of past sea-surface conditions. Our results replicate and extend late Holocene reconstructions from the Garrison Basin, using which we then create composites of SST and $\delta^{18}O_{sw}$. We find considerable centennial and millennial-scale variability in both SST and $\delta^{18}O_{sw}$, although their evolution over the Holocene is distinct. Whereas mean-annual SSTs display pronounced millennial-scale variability, $\delta^{18}O_{sw}$ exhibits a secular trend spanning multiple millennia and points to increasing northwestern GoM surface salinity since the early Holocene. We then synthesize the available Holocene records from across the GoM and alongside the Garrison Basin composite uncover substantial, yet regionally consistent, spatiotemporal variability. Finally, we discuss the role of the Loop Current and coastal influx of freshwater in imposing these heterogeneities. We conclude that dynamic surface-ocean changes occurred across the GoM over the Holocene.

Plain Language Summary The Gulf of Mexico (GoM) is a major moisture source for a significant part of North America and is an important region for ocean circulation in the North Atlantic. However, we do not have a clear picture of how temperature and salinity in the GoM varied since the advent of agriculture ~11,700 years ago (the period known as the Holocene). This has proven to be a barrier in addressing questions related to natural modes of regional precipitation and circulation variability over long timescales (centuries to thousands of years). In this work, we measure chemical signals preserved in microfossil plankton shells from sediment cores in the Garrison Basin (northwest GoM) to unravel a well-resolved Holocene history of GoM temperature and salinity variations. We then compile previously generated data across the GoM and piece together the principal climatic and oceanic drivers responsible for the observed patterns. We conclude that GoM paleoceanography across the Holocene was dynamic and complex, wherein more highly resolved records (as in this study) are needed for a more detailed picture of its spatial variability. Treating the GoM as one monolithic entity with uniform changes in its parameters across time and space is not necessarily a sound assumption.

1. Introduction

The Gulf of Mexico (GoM) is a climatically important semi-enclosed oceanic body situated at the northwestern flank of the tropical Atlantic Ocean. As a moisture source for a substantial part of the North American continent, surface-ocean conditions in the GoM exert a significant influence on climate in the United States of America, Mexico, and regions in Central America and the Caribbean. The GoM is a major component of the Atlantic Warm Pool, which is characterized by seasonal sea-surface temperatures (SST) warmer than 28.5°C (Wang & Enfield, 2003). Small changes in the onset and spatial extent of the Atlantic Warm Pool can induce large-scale changes in moisture convergence and poleward heat transport in the Western

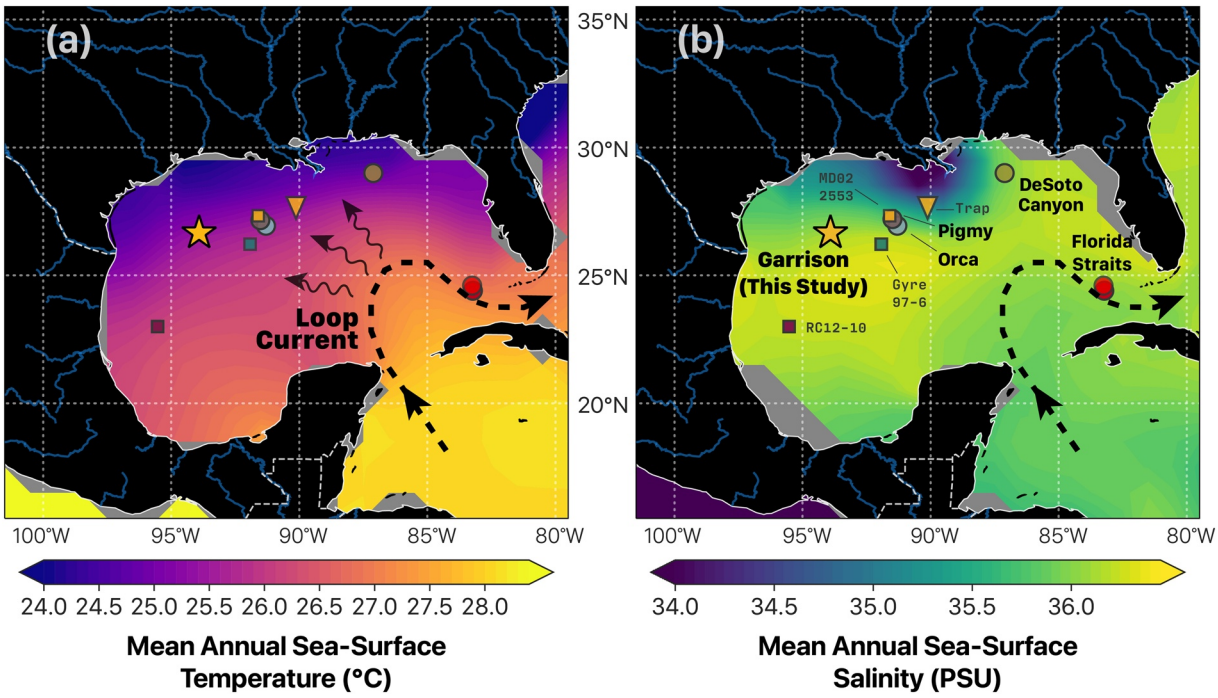

Figure 1. Modern Surface-Ocean Conditions in the Gulf of Mexico. Mean annual (a) sea-surface temperature (SST) and (b) salinity (SSS) in the Gulf of Mexico (GoM) over 1958–2014, with black lines depicting the average position of the Loop Current (a) and general direction of eddy-shedding. Marine sediment core sites of previous geochemical reconstructions are depicted with circles alongside the names of their regions or basins whereas those locations with foraminiferal species assemblage reconstructions are shown using squares with core names in fixed-width (b). Garrison Basin, the focus of this study (2010-GB2-GC1 & the stacked 2010-GB2-MCX record from Thirumalai et al., 2018) is depicted with a yellow star and the location of the sediment trap (Richey et al., 2019) is indicated with an inverted yellow triangle. Observed SST and SSS data were taken from HadISST (Rayner et al., 2003) and ORA-S4 (Balmaseda et al., 2012) data sets, respectively. Details of the previously published paleoceanographic data sets can be found in the following studies: Florida Straits - Lund and Curry (2006); Schmidt and Lynch-Stieglitz (2011); Schmidt et al. (2012); DeSoto Canyon - Nürnberg et al. (2008); Orca Basin - LoDico et al. (2006); Pigmy Basin-Richey et al. (2007); and details for the foraminiferal species assemblage records are found in Poore et al. (2003, 2005). Note that the sharp gradients in SST and SSS, which are facilitated by the interplay between Loop Current intrusion into the Gulf and freshwater runoff from North American rivers impose significant spatial variability in mean-annual conditions across the GOM, and thus among existing core locations.

Hemisphere (Misra et al., 2014; Zhang et al., 2014). Patterns of SST in the GoM can also impact the intensity of extreme events by modulating the moisture-bearing potential of low-level jets as well as hurricane activity (Algarra et al., 2019; Leipper & Volgenau, 1972). Thus, regional climates across large parts of the North American continent are intricately tied to surface-ocean properties of the GoM.

Modern GoM oceanography is dynamic and variable. The Loop Current is its principal feature and is responsible for routing warm Caribbean waters into the GoM through the Yucatán Channel and out through the Florida Straits (Liu et al., 2012; Sturges & Leben, 2000). At times, the Loop Current intrudes northwards into the northeastern GoM, sometimes up to the shelf-break on the continental slope and overall exhibits large spatial variability in its meridional position (Brokaw et al., 2019; Candela et al., 2019). Additionally, sizable (~400 km diameter) and long-lived (lasting up to a year) eddies irregularly pinch off from the Loop Current and penetrate into the GoM (Candela et al., 2019; Sturges & Leben, 2000). These eddies have distinct SST, sea-surface salinity (SSS), and nutrient concentrations relative to the surrounding waters of the interior GoM and thus impact the marine environment and its ecosystems (Brokaw et al., 2019; Liu et al., 2012). On the other hand, coastal processes including substantial freshwater discharge from the Mississippi-Atchafalaya, Rio Grande, and several smaller river systems dominate variability along the GoM coastline (Brokaw et al., 2019; Morey et al., 2003; Schiller & Kourafalou, 2014). Despite strong seasonal variability, the imprint of the Mississippi-Atchafalaya system is readily observed in the mean salinity field across the northern GoM (Figure 1). Subsequently, the interplay between the Loop Current, eddy-shedding, and coastal processes induces significant oceanographic variability across the GoM.

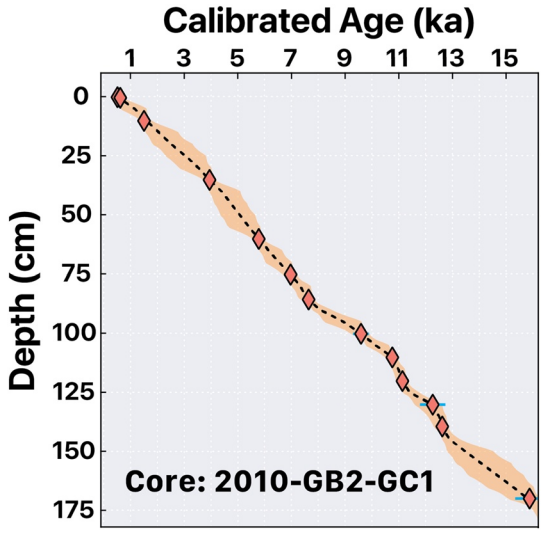

Figure 2. Age Model for 2010-GB2-GC1. Posterior calibrated ages (orange diamonds are weighted-means) and uncertainty distributions (orange envelope) from the BACON age-modeling software (Blaauw & Christen, 2011). Analytical ^{14}C errors are depicted using blue errorbars (although in most cases, they are too small to be visible behind the markers.) Samples for radiocarbon measurements consisted of pristine specimens of upper-ocean planktic foraminiferal species including *Globigerinoides ruber*, *Trilobatus sacculifer*, *Globigerinoides conglobatus*, and *Orbulina universa*. We applied the Marine13 curve (Reimer et al., 2013) to calibrate for marine reservoir ages and used a correction of −32 ± 25 years, based on ^{14}C measurements on corals from the nearby (~100 km) Flower Garden Banks Sanctuary (Wagner et al., 2009). Sedimentation rates are nearly constant at 12.5 ± 3 cm/kyr, similar to previous investigations in the Garrison Basin, northwestern GoM (Thirumalai et al., 2018).

Circulation in the GoM is tied to large-scale North Atlantic oceanography. Flows through the GoM and Caribbean regions are a part of the North Atlantic Subtropical gyre system (Candela et al., 2019; Lin et al., 2010; Liu et al., 2012; Sturges & Leben, 2000). As a precursor to the Gulf Stream through the Florida Straits, the Loop Current and its eddy-shedding processes are integrally linked to low-to-high latitude transport in the Atlantic Ocean by two mechanisms: (a) the wind-driven circulation in the North Atlantic and (b) the density-driven surface limb of the Atlantic Meridional Overturning Circulation (Candela et al., 2019; Lin et al., 2010; Liu et al., 2012). As such, anomalies in the low-latitude Atlantic can have downstream advective impacts on subtropical gyre circulation and poleward transport particularly on timescales of decades to centuries (Lin et al., 2010; Liu et al., 2012; Zhang et al., 2014). Accordingly, there is a broad interest in understanding inherent variations in these circulation systems, with particular relevance for future implications.

Marine sediments from the GoM have been the focus of extensive work investigating long-term climatic variations in the region. A plethora of Pleistocene studies have explored the paleoceanographic history of the GoM (Flower & Kennett, 1990; Kennett & Huddlestun, 1972; Leventer et al., 1982; Sackett & Rankin, 1970; Montero-Serrano et al., 2010; Nürnberg et al., 2008; Schmidt & Lynch-Stieglitz, 2011), with many seeking to constrain the routing and dynamics of glacial-aged meltwater from the Laurentide Ice Sheet (Aharon, 2006; Broecker et al., 1989; Vetter et al., 2017; Williams et al., 2012). However, few studies have examined paleoceanographic variability in the GoM over the Holocene epoch (Poore et al., 2003, 2004). Well-resolved reconstructions of Holocene climate change can establish important baselines to separate forced responses from internal variability and can inform comparisons with climate simulations. Although there are some high-resolution geochemical records concentrated in the late Holocene (Lund & Curry, 2006; Richey et al., 2007, 2009; Thirumalai et al., 2018) and a few in the early Holocene (LoDico et al., 2006; Schmidt et al., 2012), continuous and quantitative reconstructions of surface-ocean conditions in the GoM over the full epoch are lacking. This deficit has restricted efforts to delineate mechanisms involved in regional paleoclimate changes as well as shifts in low-latitude circulation across the Atlantic (Metcalfe et al., 2015).

In this work, we present surface-ocean reconstructions of the GoM over the Holocene. We developed sub-centennial-scale records of SST and the stable oxygen isotope composition ($\delta^{18}O$) of seawater ($\delta^{18}O_{sw}$; a proxy for SSS) using planktic foraminiferal geochemistry in sediments from the Garrison Basin, northwestern GoM. We then use our new data set. alongside replicated late Holocene reconstructions from the same basin (see Thirumalai et al., 2018) to create a composite record spanning the past ~11,700 years. We then synthesize the available records across the GoM to investigate spatiotemporal trends over the Holocene. Finally, we discuss the implications of the Garrison Basin composite and the compilation of GoM records on regional and North Atlantic paleoceanography.

2. Methods

2.1. Materials and Foraminiferal Proxy Approach

We used planktic foraminiferal geochemistry to reconstruct Holocene SST and $\delta^{18}O_{sw}$ variations in the northwestern GoM. Marine sediment core 2010-GB2-GC1 was raised from the Garrison Basin (26.67°N, 93.92°W) at a water depth of 1,776 m (Figure 1) aboard the R/V Cape Hatteras in April 2010. An age model was built using a Monte Carlo approach on the Bayesian posterior ages from 15 radiocarbon measurements on upper-ocean planktic foraminifera (Blaauw and Christen, 2011; Figure 2). Resultant averaged

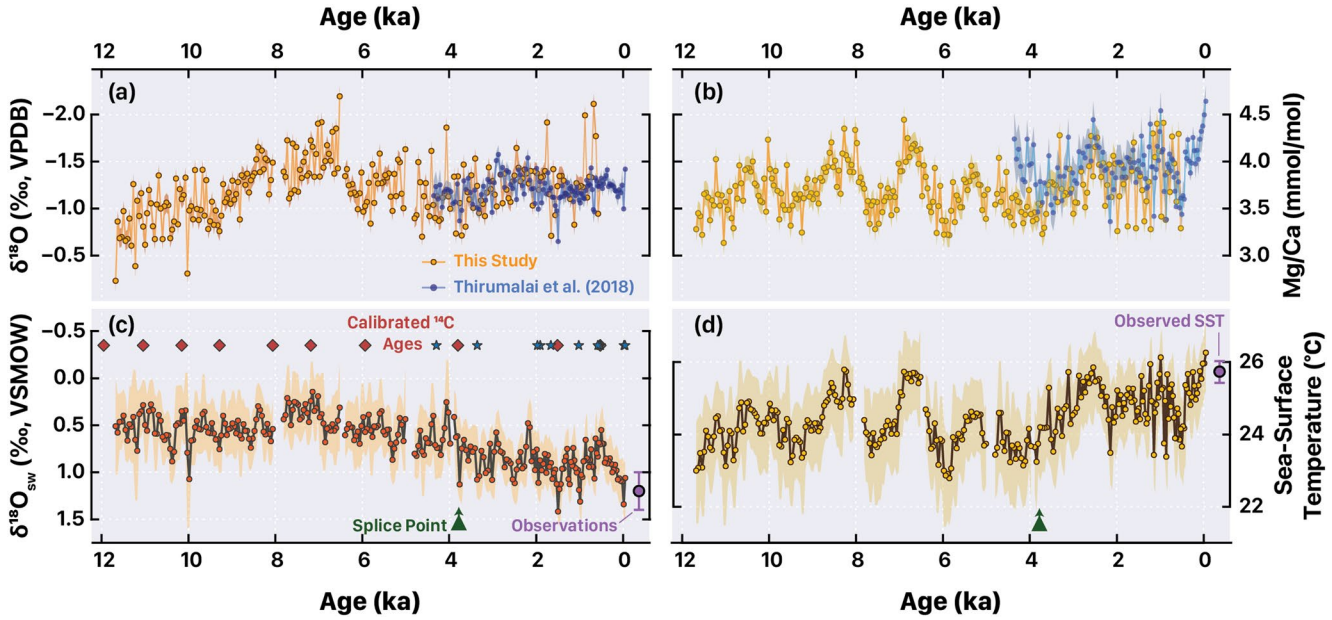

Figure 3. Surface-ocean Reconstructions from the Garrison Basin, Northern Gulf of Mexico using the Geochemistry of Planktic Foraminifera *Globigerinoides ruber*. (a–b) Multi-test measurements (n_{tests} = 70–100) of (a) the stable oxygen isotope composition ($\delta^{18}O$; reported in ‰ VPDB) and (b) trace element magnesium-to-calcium (Mg/Ca; mmol/mol) ratios in *G. ruber* from 2010-GB2-GC1 (orange; this study) and 2010-GB2-MCX (blue; Thirumalai et al., 2018), alongside (c-d) composite reconstructions of (c) seawater-$\delta^{18}O$ ($\delta^{18}O_{sw}$; reported in ‰ VSMOW), and (d) sea-surface temperature (SST); °C estimated using PSU Solver (Thirumalai et al., 2016). The composites were created by splicing the stacked multi-core reconstruction to the longer reconstruction from 2010-GB2-GC1 (this study) at ~4 ka (indicated by the splice point). Observed $\delta^{18}O_{sw}$ (c) and mean-annual SST (d) at the site are depicted in purple where errorbars are the standard deviation in available $\delta^{18}O_{sw}$ measurements (see Thirumalai et al., 2018) and in mean-annual SST over 1970–2010 from the HadiSST data set (Rayner et al., 2003), respectively. Calibrated radiocarbon ages for the 2010-GB2-GC1 (red diamonds) and the stacked multi-core reconstruction (blue stars) are also shown. Note strong degree of replication between the measurements of both records.

sedimentation rates of 12.5 ± 3 centimeters (1σ) per thousand years (cm/kyr) are consistent with earlier investigations in the Garrison Basin (Thirumalai et al., 2018). The core-top of 2010-GB2-GC1 was dated to ~530 years before present (BP); relative to 1950 C.E. Sedimentary mixed layers are typically <5 *cm* along the GoM continental slope, and a previous bioturbation analysis for the Garrison Basin demonstrates that sub-centennial-scale resolution foraminiferal records can reliably capture centennial to multi-centennial climatic signals (Thirumalai et al., 2018).

We measured the $\delta^{18}O$ (n = 265) and magnesium-to-calcium (Mg/Ca) ratio (n = 275) composition in the calcareous shells of the white variety of planktic foraminifera *Globigerinoides ruber* (hereafter *G. ruber*) (Figure 3). Reconstructions using *G. ruber* in the northwestern GoM reflect mean-annual conditions in the upper ~50 m (Richey et al., 2019; Thirumalai et al., 2014, 2018). For this study, we did not discriminate between different morphotypes of *G. ruber*, as we have previously demonstrated their equivalency for reconstructions of Holocene climate in the GoM (Thirumalai et al., 2014). We do acknowledge, however, that other studies have found varying environmental sensitivities between the two morphotypes in various regions including their seasonal occurrence and depth of calcification (Carter et al., 2017; Steinke et al., 2005; Wang, 2000). Interestingly, Antonarakou et al. (2015) found downcore differences in Mg/Ca-SSTs derived from different *G. ruber* morphotypes across the last deglacial transition in the GoM, although, we note that their sampling resolution was low (~millennial-scale) and moreover they used rather small numbers of specimens per sample (15–20 individuals). In our work, we picked 70–100 individual shells from 0.5 cm sediment intervals (corresponding to an average time resolution of ~45 years per sample) after which they were gently crushed and homogenized. A large fraction of this mixture was kept aside for trace metal analysis whereas the remnant portion was used for stable isotope analysis, which was performed on an isotope ratio mass spectrometer housed at the University of Texas at Austin. All $\delta^{18}O$ values are reported in permil notation relative to the Vienna Pee Dee Belemnite scale (‰, VPDB). Based on an external standard, NBS-19 (n = 89), the 1σ analytical precision was ±0.03‰ for $\delta^{13}C$ and ±0.06‰ for $\delta^{18}O$, consistent with the

long-term precision of the instrumental setup (0.06‰ for $\delta^{13}C$ and 0.08‰ for $\delta^{18}O$). Note that reconstructed and observed $\delta^{18}O_{sw}$ values are reported in permil notation relative to the Vienna Standard Mean Ocean Water scale (‰, VSMOW).

Elemental ratios were measured at the USGS Coastal and Marine Science Center following established foraminiferal cleaning techniques (Barker et al., 2003; note that we did not use the reductive cleaning step). Mg/Ca analysis was performed using inductively coupled plasma optical emission spectrometry utilizing protocols similar to those reported in Thirumalai et al. (2018) following Schrag (1999). Along with an internal gravimetric standard which was used to monitor drift and precision, repeat measurements on external, matrix-matched standards yielded an analytical precision of ±0.15% (1σ = 0.02 mmol mol^{-1}). We inferred sampling uncertainty from replicate measurements of different sets of *G. ruber* tests from the same sample depth (n = 30), which was ±3% (0.10 mmol/mol) and ±0.08‰, respectively, for Mg/Ca and $\delta^{18}O$ analysis. Both analytical and sampling uncertainty were taken into account while computing SST and $\delta^{18}O_{sw}$.

The procedure and uncertainty associated with using paired $\delta^{18}O$-Mg/Ca measurements on planktic foraminifera to estimate SST and $\delta^{18}O_{sw}$ variability is well-documented. Many recent studies have refined quantitative temperature estimates stemming from Mg/Ca paleothermometry and detail the impact of propagating uncertainties on the ensuing reconstructions (Arbuszewski et al., 2010; Gray et al., 2018; Hertzberg & Schmidt, 2013; Holland et al., 2020; Khider et al., 2015; Saenger & Evans, 2019; Thirumalai et al., 2016; Tierney et al., 2019). Studies have also demonstrated that secondary influences of pH and salinity can significantly affect foraminiferal Mg/Ca variations (Arbuszewski et al., 2010; Gray & Evans, 2019; Gray et al., 2018; Kısakürek et al., 2008; Lea et al., 1999; Mathien-Blard & Bassinot, 2009; Nürnberg et al., 1996; Sadekov et al., 2009). Here, we used the Paleo-Seawater Uncertainty Solver (PSU Solver) uncertainty propagation algorithm (Thirumalai et al., 2016) to probabilistically constrain surface-ocean temperature and $\delta^{18}O_{sw}$ variability over the Holocene from our paired Mg/Ca-$\delta^{18}O$ measurements. PSU Solver probabilistically inverts for SST, SSS, and $\delta^{18}O_{sw}$ and their respective uncertainties for a given set of paired Mg/Ca and $\delta^{18}O$ foraminiferal measurements. Using user-specified sets of equations, PSU Solver utilizes a bootstrap Monte Carlo procedure to propagate error and invert for the aforementioned parameters (Thirumalai et al., 2016). For this work, we applied the following equations in PSU Solver to invert for SST and local $\delta^{18}O_{sw}$: the culture-based Mg/Ca equation outlined in Tierney et al. (2015), the culture-based $\delta^{18}O$ ("low-light") relationship from Bemis et al. (1998), and the "North Atlantic" $\delta^{18}O_{sw}$-salinity relationship from LeGrande and Schmidt (2006). This combination has been previously shown to yield accurate comparisons of core-top measurements with observations in the Garrison Basin (Richey et al., 2019; Thirumalai et al., 2018). The Mg/Ca equation is built using data from a series of planktic foraminiferal culture experiments (Dueñas-Bohórquez et al., 2011; Hönisch et al., 2013; Kısakürek et al., 2008; Nürnberg et al., 1996) and explicitly accounts for the influence of salinity on Mg/Ca variability. We note that this combination has been validated by comparing observations with foraminiferal measurements from a nearby sediment trap in the northern GoM (Richey et al., 2019; Figure 1). We further note that this combination slightly outperforms a more recent calibration equation (Gray et al., 2018) while comparing core-top values with observations of temperature and $\delta^{18}O_{sw}$ in the Garrison Basin (see Figure S1), consistent with the sediment trap results (Richey et al., 2019). Our procedure also accounts for variations in global ice volume (and hence, global sea level), a parameter which can influence global oceanic $\delta^{18}O_{sw}$ composition, independent of changes in local hydrography and salinity (Thirumalai et al., 2016). Although these variations were not as large in the Holocene relative to the glacial period, they can still significantly influence inversions (~0.3–0.5‰) of local $\delta^{18}O_{sw}$ and thus, we employed a recent sea-level curve for the deglaciation and Holocene (Lambeck et al., 2014) to account for this effect. We note that this sea-level curve is highly resolved and provides improved estimates relative to other curves (Thirumalai et al., 2016).

2.2. The Garrison Basin Composite Record

We constructed a composite Holocene record of SST and local $\delta^{18}O_{sw}$ for the Garrison Basin. Previously, Thirumalai et al. (2018) presented stacked surface-ocean records (also using paired measurements on white *G. ruber*) from the Garrison Basin spanning the past ~4.2 kyrs. These records were based on measurements from three multi-cores (2010-GB2-MCA/MCB/MCC; hereafter 2010-GB2-MCX), which contained intact

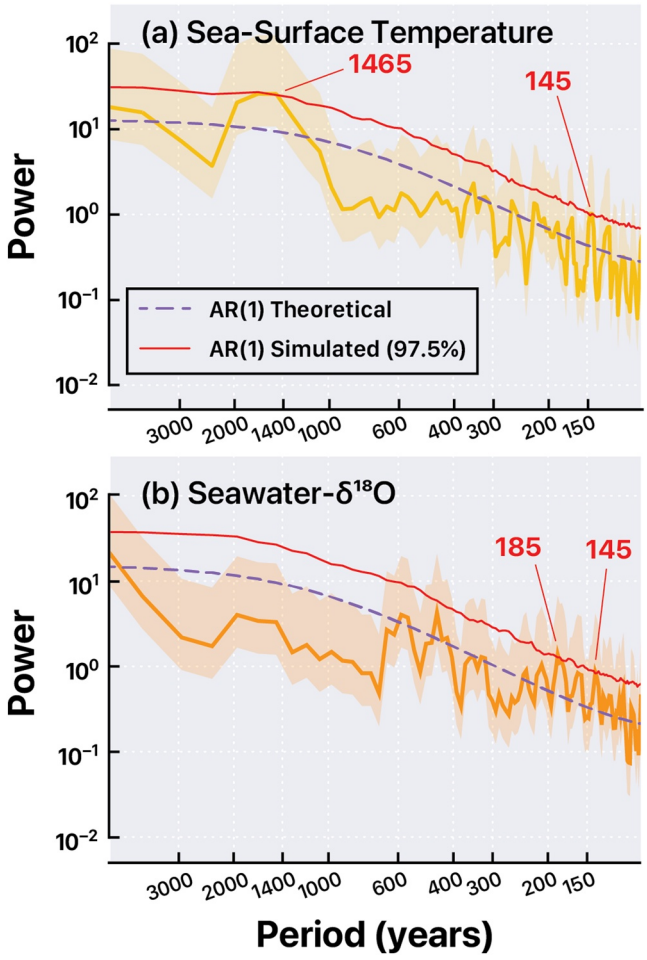

Figure 4. Spectral Characteristics of the Composite Reconstructions from the Garrison Basin, Northwestern Gulf of Mexico. Multi-taper spectra for the composite (a) sea-surface temperature (SST) and (b) seawater-δ^{18}O ($\delta^{18}O_{sw}$) reconstructions from the Garrison Basin, with median (thick lines) and 95% ($\pm 2\sigma$) confidence level envelopes (estimated from a χ^2 distribution). Statistical significance was determined against a first-order autoregressive (AR-1) red-noise null hypothesis, where totally, two significant peaks (red numbers) were found in SST (145-year & 1465-year periodicity) and seawater-δ^{18}O (145-year & 185-year periodicity) each at the 97.5% confidence level. Note lack of lower-frequency (>~600-year periodicity) variance in the $\delta^{18}O_{sw}$ spectrum.

and modern core-tops. A comparison between the raw Mg/Ca and δ^{18}O values in the multi-core stack and those in 2010-GB2-GC1 spanning from ~11.7 ka to ~0.5 ka is presented in Figures 3a and 3b. To create a continuous record across the entire Holocene and to take advantage of the additional age constraints and the relatively unperturbed nature of the younger multi-cores, we spliced together the stacked SST and local $\delta^{18}O_{sw}$ reconstructions till ~4 ka with those developed from 2010-GB2-GC1 (this study; see Figure 3). Consequently, the core-tops of the composited records compare well with observed SST from the HadISST data set (Rayner et al., 2003) and measured $\delta^{18}O_{sw}$ in the GoM (Thirumalai et al., 2018; Figures 3c and 3d). The ensuing spliced reconstructions are hereafter referred to as the Garrison Basin composite records. Spectral analysis was performed on these composite records using a multi-taper methodology ($n_{tapers} = 3$) with uncertainty estimated from a χ^2 distribution and where significance was assessed against a red-noise hypothesis using a first-order autoregressive (AR1) process (Figure 4). Regressions were calculated using bivariate errors in a maximum likelihood framework (Thirumalai et al., 2011), and the probability of onset for trends was estimated using a Bayesian change point methodology (Ruggieri, 2012).

2.3. Compilation of Holocene Paleoceanographic Records in the GoM

To investigate regional Holocene paleoceanography in the GoM, we compiled available foraminiferal reconstructions of surface-ocean variability (Figures 5–7). These included reconstructions of relative population abundances of foraminiferal species (square markers in Figure 1) from the northwestern (Poore et al., 2005: MD02-2553; Poore et al., 2003: Gyre97-6) and western GoM (Poore et al., 2003: RC12-10) along with geochemical reconstructions (circle markers in Figure 1) from the Pigmy Basin (Richey et al., 2007), Orca Basin (LoDico et al., 2006; Williams et al., 2012), DeSoto Canyon (Nürnberg et al., 2008), and the Dry Tortugas' side of the Florida Straits (Lund & Curry, 2006; Schmidt et al., 2012). We also reprocessed the original radiocarbon measurements with the BACON algorithm to generate updated age-model constraints in each of these records (Blaauw & Christen, 2011). We performed principal component analysis (PCA) for the three records of species assemblages, which included 18 taxa of planktic foraminifera each, and grouped them based on their co-variance (Figure 7). Correlations between the principal components and the Garrison Basin records were found after interpolating both to the same time step. For the geochemical compilation, we selected records from studies which also used paired δ^{18}O-Mg/Ca measurements of *G. ruber* and similarly transformed them into mean-annual SST and $\delta^{18}O_{sw}$ using PSU Solver. We applied the same set of equations as indicated above in PSU Solver for these records as well, except for those from the Florida Straits wherein the "Tropical Atlantic" (instead of "North Atlantic") $\delta^{18}O_{sw}$-salinity relationship was employed due to more accurate core-top comparisons with observations. We note that these specific sets of equations were chosen as they yielded accurate core-top SST and $\delta^{18}O_{sw}$ values which compare well with observations (Figures 5 and 6). To create a Holocene-long composite for the Florida Straits, we spliced together three nearby paired records proximal to the Dry Tortugas (after independently transforming them into SST and local $\delta^{18}O_{sw}$) spanning from ~12–9.4 ka (Schmidt and Lynch-Stieglitz, 2011: KNR166-2-26JPC), ~9.1–1.5 ka (Schmidt et al., 2012: KNR166-2 JPC 51), and 1.1–0 ka (Lund and Curry, 2006: W167-79GGC). Ultimately, comparisons with these geochemical and relative population abundance records were used to address spatiotemporal variability across the GoM over the Holocene.

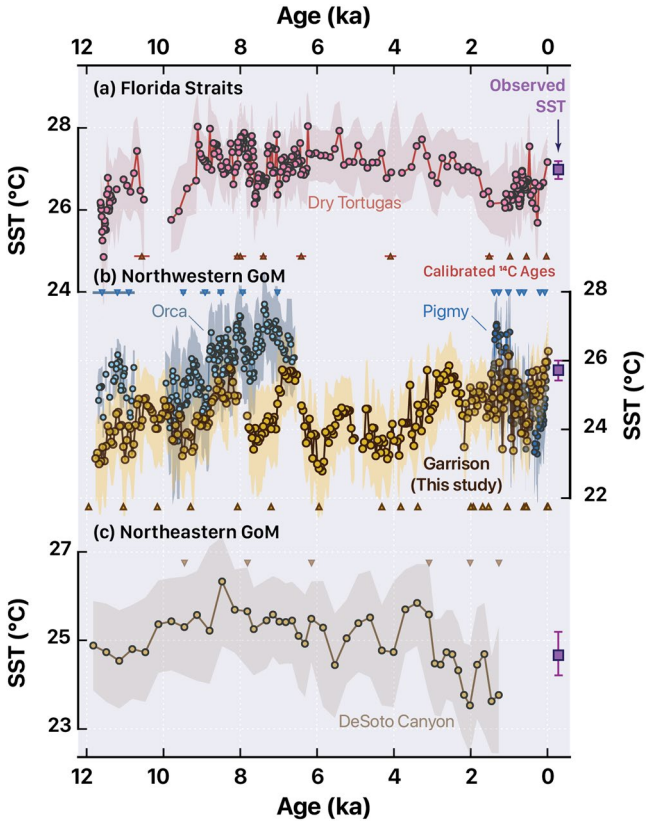

Figure 5. Holocene Sea-Surface Temperature Variability in the Gulf of Mexico. Sea-surface temperature (SST) reconstructions from (a) the Florida Straits with SST composite created from records (Lund & Curry, 2006; Schmidt & Lynch-Stieglitz, 2011; Schmidt et al., 2012) near the Dry Tortugas (see Methods for details), (b) the northwestern Gulf of Mexico (GoM) consisting of records from the Garrison Basin (this study, spanning the entire Holocene), the Orca Basin (12–6 ka; LoDico et al., 2006), and the Pigmy Basin (2–0 ka; Richey et al., 2007), and (c) the northeastern GoM with a record from DeSoto Canyon (Nürnberg et al., 2008). Modern observations of mean-annual SST at each location are indicated by the purple squares (error bars indicate standard deviation over 1970–2010; SST was taken from HadISST, Rayner et al., 2003). Reconstructions at all sites are based on paired measurements of δ^{18}O and Mg/Ca in *G. ruber* with uncertainty estimates computed using PSU Solver (Thirumalai et al., 2018; see Methods for details).

3. Results and Discussion

3.1. Garrison Basin Composite SST & $\delta^{18}O_{sw}$

The Garrison Basin SST composite indicates that the northwestern GoM experienced large millennial-scale temperature swings over the Holocene. Core-top SST in the composite agrees (within uncertainty) with mean-annual SST observations (Figure 3d) and indicates that modern temperatures are relatively higher than most of the Holocene. However, four periods of distinct warmth equivalent to modern temperatures (within uncertainty) are also observed. These include periods between 8.5–8.2 ka, 6.8–6.5 ka, 2.7–2.4 ka, and 1.2–0.8 ka (Figure 3d). Warmth similar to modern conditions in the northwestern GoM during 8.5–8.2 ka (occurring before or coincident with the "8.2 kyr event") and 1.2–0.8 ka (proximal in time to the purported "Medieval Climate Anomaly") have also been documented previously (LoDico et al., 2006; Richey et al., 2007). Relatively cool SSTs prevailed from 9.5–9.2 ka, 7.7–7.3 ka, 6–5.8 ka, 4.4–4.1 ka, and as shown before, during 0.5–0.3 ka (Thirumalai et al., 2018; "Little Ice Age"). According to the composite, the northwestern GoM experienced its coolest SSTs of the Holocene at ~6 ka. The transitions between these periods follow a quasi-oscillatory pattern and are interspersed by 1–2 millennia in the early to mid-Holocene, which eventually become more varied in the late Holocene. Smaller in magnitude than the millennial-scale oscillations (which are on the order of ~1 °C/kyr), a significant, multi-millennial warming trend (~0.3 °C/kyr; $r^2 = 0.3$, $p < 0.01$) is observed beginning at ~4 ka (change point probability for onset of trend is 10% wherein those for the larger oscillations are ~50%–60%).

Additionally, we find significant periodicities at 1465 years and 145 years in the spectra of the Garrison Basin composite SST record (Figure 4a). The shorter peak is consistent with pronounced centennial-scale variability also uncovered in previous investigations (Thirumalai et al., 2018). We are confident that these centennial-scale periodicities in the composite record are not artifacts, as we also find them in the spectra of the 2010-GB2-GC1 records independent from the late Holocene stack (not shown). The longer period of 1465 years is similar to millennial-scale periodicities found in other records across the North Atlantic Ocean (Wanner et al., 2011, 2015). These quasi-periodic ~1500-year oscillations are sometimes referred to as "Bond cycles" after Bond et al. (2001), who documented the cyclic nature of ice-rafted debris in North Atlantic sediments over the Holocene. Volcanic glass and hematite-stained grains found in these sediments were interpreted as episodic incursions of ice-bearing waters from the Nordic and Labrador Seas into the North Atlantic which subsequently weakened thermohaline circulation in the region (Bond et al., 2001; Wanner et al., 2015). It was also posited that variations in solar activity caused the southward advection of meltwater and the subsequent cooling of the Northern Hemisphere over the Holocene (Bond et al., 2001; Wanner et al., 2011). To investigate the imprint of Bond cycles in our SST reconstruction, we correlated the Garrison Basin SST record with the North Atlantic drift-ice stack of Bond et al. (2001), as well as the Total Solar Irradiance (TSI) reconstruction from Steinhilber et al. (2012) (Figure S2). This exercise showed that the Garrison Basin SST record bears little-to-no statistical correspondence with either TSI reconstruction ($r^2 = 0.04$; $p > 0.05$) or North Atlantic drift-ice variability over the Holocene ($r^2 = 0.1$; $p > 0.05$). Thus, neither solar activity nor Bond cycles provide a simple explanation for the origin of the 1465-year SST periodicity at our site. Although the northern GoM was one of the major sinks of glacial-era meltwater routing, this lack of correlation could imply that Bond cycles in the Holocene are decoupled from meltwater drainage through the Mississippi, and potentially more sensitive to outflows in the subpolar Atlantic Ocean. In sum, Holocene

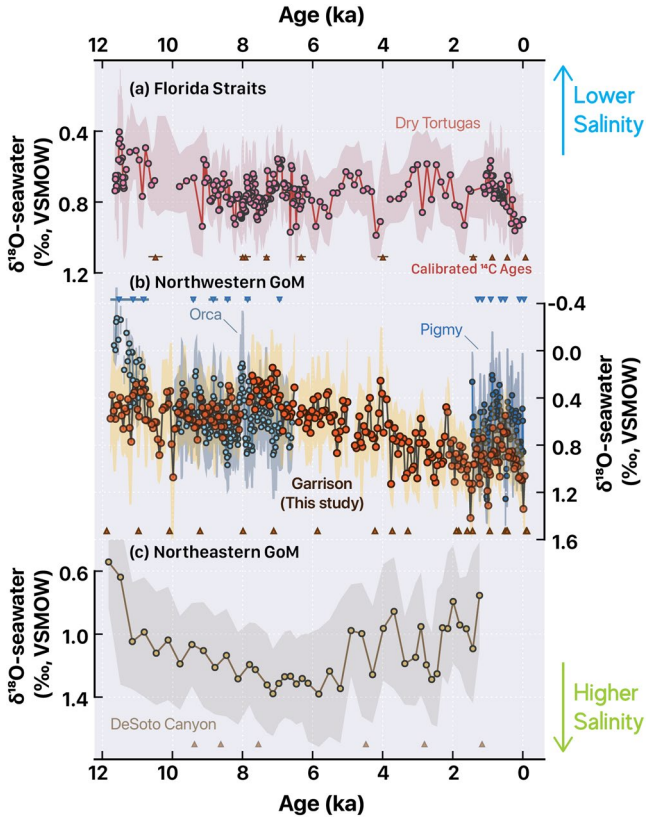

Figure 6. Surface-Ocean Seawater-$\delta^{18}O$ Variability in the Gulf of Mexico over the Holocene. Reconstructions of the upper-ocean stable oxygen isotope composition of seawater ($\delta^{18}O_{sw}$; a proxy for salinity) from (a) the Florida Straits with a composite created from cores proximal to the Dry Tortugas (Lund and Curry, 2006; Schmidt and Lynch-Stieglitz, 2011; Schmidt et al., 2012; see Methods for details), (b) the northwestern Gulf of Mexico (GoM) consisting of records from the Garrison Basin (this study, spanning the entire Holocene), the Orca Basin (12–6 ka; LoDico et al., 2006), and the Pigmy Basin (2–0 ka; Richey et al., 2007), and (c) the northeastern GoM with a record from DeSoto Canyon (Nürnberg et al., 2008). Reconstructions at all sites are based on paired measurements of $\delta^{18}O$ and Mg/Ca in *G. ruber* with uncertainty estimates computed using PSU Solver (Thirumalai et al., 2018; see Methods for details).

SSTs in the Garrison Basin exhibited substantial centennial-scale variability superimposed on millennial-scale oscillations that do not appear to be clearly linked to external solar forcing or North Atlantic drift ice.

The composite $\delta^{18}O_{sw}$ record from the northwestern GoM is characterized by a secular trend with muted millennial-scale variability. Local (ice-volume corrected) $\delta^{18}O_{sw}$ at Garrison Basin shows relatively uniform values from the beginning of the Holocene until ~8 ka, with considerable centennial-scale fluctuations (Figure 3c). Starting at ~8–7.5 ka (change point probability ~60%), $\delta^{18}O_{sw}$ becomes more positive, increasing from 0.3‰ (VSMOW) to 1.1‰ at a rate of 0.09‰ per kyr ($r^2 = 0.6$, $p < 0.01$). Eventually, in the late Holocene from ~4 ka onwards, the trend becomes less steep (0.05‰ per kyr; $r^2 = 0.2$, $p < 0.01$).

Early Holocene SSS values in the northwestern GoM were much lower than modern values. According to the $\delta^{18}O_{sw}$-salinity relationship from LeGrande and Schmidt (2006) (consistent with validation exercises; see Richey et al. (2019) for details), this trend amounts to an increase of ~ 1 psu over the past 8 kyr, from ~35.3 psu at 8–7 ka to a mean value of ~ 36.3 psu over the last millennium (c.f., mean-annual SSS at the Garrison Basin site from the ORA-S4 reanalysis data set (Balmaseda et al., 2012) is 36.4 psu from 1970–2010). During this latter period, there is a brief return to fresher conditions, coincident with the "Little Ice Age" (Thirumalai et al., 2018). Such episodic low-salinity excursions are also found at 7.1–7.0 ka, 4.1–4.0 ka, 2.9 ka, and 2.2–2.1 ka. Despite suppressed millennial-scale variability compared to the composite SST record, $\delta^{18}O_{sw}$ exhibits persistent centennial-scale variability throughout the Holocene (Figure 3c). We also found no straightforward relationship between the $\delta^{18}O_{sw}$ record and solar activity or North Atlantic drift ice (not shown). Consequently, the $\delta^{18}O_{sw}$ spectra does not contain any periods in the millennial band significant against an AR1 red noise process, but, similar to the SST record contains a significant peak at 145 years (Figure 4b). Whereas the lowest $\delta^{18}O_{sw}$ values occur around 7 ka, and briefly at ~4 ka, the highest excursions (corresponding to increased salinity) all occur in the last two millennia (Figure 3c).

3.2. SST Variability in the GoM Over the Holocene

Compiled records from the GoM clearly suggest large regional heterogeneity in their Holocene temperature histories (Figure 5). We designated the Dry Tortugas' composite as a record representative of the eastern Florida Straits, the records from Orca (LoDico et al., 2006; Williams et al., 2012), Pigmy (Richey et al., 2007), and Garrison Basin (this study) as reflecting conditions across the northwestern GoM, and the lower-resolution DeSoto Canyon record (Nürnberg et al., 2008) as one recording surface oceanography in the northeastern GoM. Whereas, the Florida Straits composite record consists of records from cores proximal to each other, we stress that significant differences in mean-annual SST and SSS (including their variability) exist between the distant Orca, Pigmy, and Garrison basins. In an ideal scenario, well-resolved records spanning the Holocene would exist for all these locations. Nevertheless, we group these records under the northwestern GoM region to investigate spatial variability across the Holocene.

The composite Florida Straits record points to relatively cool conditions from 12–10 ka relative to modern temperatures with a transition toward warmer SSTs at 9 ka (Figure 5a). Temperatures during 9–8 ka are ~ 0.7°C higher than SSTs during the last millennium with a gradual decline over the Holocene (Figure 5a). Despite this decline, given the uncertainties in this record, we were unable to find a statistically significant

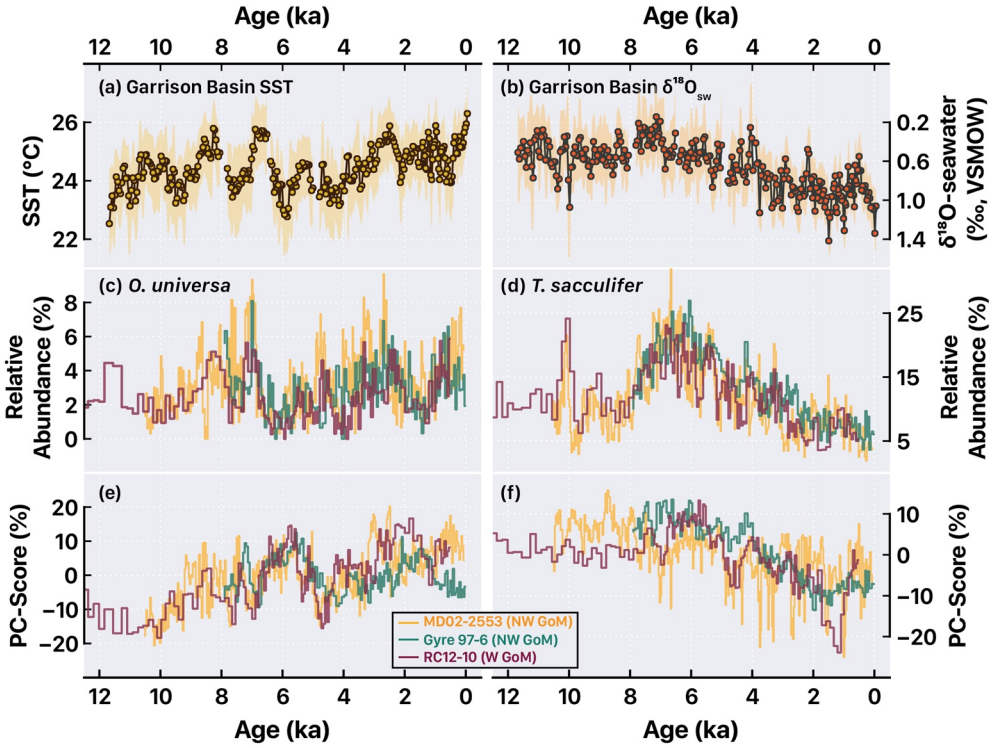

Figure 7. Comparing Holocene Paleoceanographic Records across the Western Gulf of Mexico. (a–b) Composite reconstructions of (a) sea-surface temperature (SST) and (b) seawater-$\delta^{18}O$ ($\delta^{18}O_{sw}$; a proxy for salinity) from the Garrison Basin. (c–d) The relative abundance of planktic foraminifers (c) *Orbulina universa,* and (d) *Trilobatus sacculifer* at three different core sites: MD02-2553 (yellow; Poore et al., 2005), Gyre97-6 (green; Poore et al., 2003), and RC12-10 (maroon, Poore et al., 2003). (e–f) Comparison between leading modes of variability using principal component analysis on the relative abundance of all planktic foraminiferal taxa (18 species) at each core site where (e) contains PC-1 from RC12-10 (explaining 40% of overall variance) and MD02-2553 (30%), and PC-2 from Gyre97-6 (21%), whereas (f) contains PC-2 from RC12-10 (25%) and MD02-2553 (22%), and PC-1 from Gyre97-6 (48%). These PCs were grouped to reflect similarities between themselves and based on their correspondence with the Garrison Basin composite reconstructions.

trend from 8 ka to the present. Though some centennial-scale variability is evident in this composite, the lack of continuous high-resolution sampling in this record inhibits a more detailed look.

In the northwestern GoM, the shorter SST records from the Pigmy and Orca Basins align fairly well with the Garrison Basin composite (Figure 5b). Though Orca Basin SSTs are higher than in the Garrison Basin record (note that mean-annual SST is warmer in the Orca Basin today by ~0.5°C), they share similar millennial-scale variability. Both the records exhibit a pronounced warming from 10–8 ka and show relatively abrupt cooling around ~8 kyrs ago. A mismatch occurs at ~7.3 ka when the Orca Basin SST record abruptly warms prior to the Garrison Basin composite. More work is required to ascertain whether these misalignments arise due to age-related uncertainty (note lack of age control in the Orca record during peak warmth), or if trace metal geochemistry was affected by the onset of anoxic conditions associated with brine lake formation in the Orca Basin at ~8 ka (Pilcher & Blumstein, 2007). Late Holocene SST variability from the Pigmy Basin is more in line with those in the Garrison Basin composite albeit with slightly warmer values from 1.5–1 ka (note that modern mean-annual SST at the Pigmy Basin is ~0.5°C higher).

The lower-resolution DeSoto Canyon record suggests relatively uniform temperatures in the northeastern GoM, with minor centennial-scale SST variability over much of the Holocene. Similar in timing to the northwestern GoM, this record also indicates warming in the northeastern GoM from 10–8 ka (Figure 5c). After comparatively stable conditions (within uncertainty) from 8–3 ka, a short cooling trend is observed from ~3 ka (change point probability ~10%) till the core-top, which is dated at 1.2 ka. Interestingly, this cooling trend coincides in its onset with a warming trend in the Garrison Basin record (Figures 5b and 5c),

although the lower resolution and age control in the DeSoto Canyon record inhibits a more detailed comparison. No other statistically significant trends were found in the DeSoto Canyon SST record over the Holocene.

We observe large spatiotemporal variability in GoM SSTs across the Holocene. We infer that our compiled records represent mean-annual SST conditions and as such do not expect (nor observe) trends mirroring changes in seasonal insolation over the Holocene. Overall SST variability across the Holocene is smaller in the Florida Straits ($1\sigma = 0.54$°C) and DeSoto Canyon record ($1\sigma = 0.63$°C) compared to the northwestern GoM ($1\sigma_{\text{Garrison}} = 0.71$°C; $1\sigma_{\text{Orca/Pigmy}} = 0.89$°C). Such a response is consistent with observed multidecadal SST variability being muted in the interior GoM (Thirumalai et al., 2018). However, the millennial-scale oscillations observed in the northwestern GoM records are not present in the other regions.

What caused regional heterogeneity in Holocene SST patterns across the GoM? We suspect that fluctuations in the Loop Current flow and its associated eddy-shedding processes might be responsible for these patterns. Among observations and general circulation models, flow through the Loop Current and the frequency of eddy shedding are positively correlated (Candela et al., 2019; Lin et al., 2010; Liu et al., 2012). In other words, stronger flow through the Loop Current is linked to a heightened propensity for eddy shedding. Thirumalai et al. (2018) showed how such processes might rectify mean-annual conditions over centennial timescales. Accordingly, we speculate that millennial-scale Holocene periods with cooler SSTs in the northwestern GoM are times of diminished Loop Current influence through reduced eddy penetration, and that the opposite occurs for the warm periods. We posit that SST gradients between the northwestern GoM and the Florida Straits are ultimately driven by flow from the Yucatán through the Florida Channel. As these processes occur on seasonal and interannual timescales (Lin et al., 2010; Liu et al., 2012), we suggest that future investigations of individual foraminiferal analyses in the GoM could stand to support or refute our hypothesis. With such analyses, we would expect larger variance during periods of warmer mean-annual SST relative to the cooler excursions, where the lack of eddy penetration in the latter would potentially suppress the annual cycle and interannual variability. Finally, as changes in seasonal insolation follow distinct trajectories over the past 12 ka due to changes in precession (i.e., half-cycle over that period), the lack of significant, secular trends in all the records suggest that the influence of orbital forcing on modulating mean-annual SSTs in the GoM over the Holocene is minimal.

3.3. $\delta^{18}O_{sw}$ Variability in the GoM Over the Holocene

Records of $\delta^{18}O_{sw}$ from the GoM indicate regionally distinct surface salinity characteristics over the Holocene. The Florida Straits composite record shows relatively lower $\delta^{18}O_{sw}$ values (~0.3 ‰ more negative than the core-top value) in the earliest part of the Holocene (12–10 ka), suggesting fresher and less saline conditions compared to today (Figure 6a). Nevertheless, $\delta^{18}O_{sw}$ remained fairly steady from ~10 ka until the last millennium in this region with centennial-to-millennial scale variability on the order of 0.1‰ (1σ). $\delta^{18}O_{sw}$ over the last millennium trends toward more positive values (i.e., higher salinity), and has been discussed in previous studies (Lund & Curry, 2006; Richey et al., 2009; Thirumalai et al., 2018). Apart from these excursions during the earliest (low $\delta^{18}O_{sw}$) and latest (high $\delta^{18}O_{sw}$) intervals of the Holocene, Florida Straits $\delta^{18}O_{sw}$ was relatively stable for most of the epoch.

The northwestern GoM records indicate a multi-millennial salinification trend over the Holocene starting around 8 ka (Figure 6b). At the Garrison Basin, mean $\delta^{18}O_{sw}$ values at 8–7 ka are ~0.5‰ less than at 1–0 ka, a magnitude which is slightly larger than the corresponding difference between mean $\delta^{18}O_{sw}$ in the Orca (early Holocene) versus Pigmy Basin (late Holocene) records (~0.3‰). It should be noted that mean-annual SSS values from observations at the Orca and Pigmy basins are lower than in the Garrison Basin due to their proximity to Mississippi-Atchafalaya outflow (Figure 1). Although Orca Basin $\delta^{18}O_{sw}$ is lower than in the Garrison Basin composite from 12–10 ka (potentially related to the influence of the waning Laurentide Ice Sheet; see Williams et al. (2012) for details), their mean values are virtually identical from ~10-7 ka. As Garrison Basin $\delta^{18}O_{sw}$ was significantly elevated compared to modern conditions, this finding suggests that the mean-annual freshwater plume from the rivers draining into the northern GoM (c.f., Figure 1) extended further into the interior GoM in the early Holocene. $\delta^{18}O_{sw}$ at the Garrison Basin gradually increases toward

modern values from the mid-Holocene. From 2–0 ka, average $\delta^{18}O_{sw}$ values at Pigmy Basin are lower than in the Garrison Basin composite, but show similar variability with a sharp decline (indicating freshening) during the middle of the last millennium (Richey et al., 2007; Thirumalai et al., 2018). The trend toward higher SSS conditions in the northwestern GoM since ~8 ka is robust and observed in the Garrison Basin composite as well as in the difference between the Orca and Pigmy basin $\delta^{18}O_{sw}$ records.

We posit that changes in the volume of riverine discharge led to increasing $\delta^{18}O_{sw}$ in the northwestern GoM over the Holocene. Significantly lower local $\delta^{18}O_{sw}$ (i.e., corrected for the impact of global ice volume on global $\delta^{18}O_{sw}$) in the early Holocene can be explained by increased freshwater input to the GoM (including local precipitation-minus-evaporation as well as runoff), the decreased advection of relatively high-salinity (and warm) eddies from the Loop Current overwhelming coastal runoff, or by a more negative shift in the isotopic end-member of the freshwater. The $\delta^{18}O_{sw}$ trend begins after ~8 ka, when global sea-level was comparatively stable and the impact of Northern Hemisphere ice-volume on global $\delta^{18}O_{sw}$ was negligible (note that all $\delta^{18}O_{sw}$ records are "ice-volume corrected" over the entire Holocene). Further, modern salinity and $\delta^{18}O_{sw}$ at the location of Garrison Basin fall in the "open ocean" cluster relative to coastal measurements and thus have reduced sensitivity to isotopic changes of the freshwater end-member (Richey et al., 2019; Wagner & Slowey, 2011; Vetter et al., 2017). Consequently, isotopic changes in riverwaters due to the waning of the Laurentide Ice Sheet are unlikely to have triggered monotonic changes in northwestern GoM $\delta^{18}O_{sw}$ well past the mid-Holocene. Moreover, we suspect a minimal contribution from long-term changes in the Loop Current and its eddy-shedding system to the multi-millennial trend of increasing $\delta^{18}O_{sw}$ values. For one, warm SSTs from 9–6 ka (Figure 5b) are consistent with an increased presence of Loop Current eddies, and therefore preclude diminished advection of Caribbean waters as an adequate cause for lower salinity in the early Holocene. Second, the lack of correlation between SST and $\delta^{18}O_{sw}$ over the full Garrison Basin composite record ($r^2 = 0.06$) points to independent controls on each parameter (Thirumalai et al., 2018). We hypothesize that increasing mean-annual salinity since the early Holocene in the northwest GoM is a direct result of diminished freshwater outflow from either the Mississippi-Atchafalaya or Rio Grande systems, or both.

Yet, our compilation suggests that salinity responses over the Holocene were not uniform across the northern GoM. In contrast to the northwestern GoM, the DeSoto Canyon record shows declining $\delta^{18}O_{sw}$ (or diminished salinity) in the northeastern GoM since the mid-Holocene. From the earliest part of the Holocene, the record exhibits a trend toward higher $\delta^{18}O_{sw}$ values till ~7 ka (0.06‰ per kyr; $r^2 = 0.8$, $p < 0.01$). After stabilizing from 7.5 to ~6 ka, there is an opposite trend toward more negative $\delta^{18}O_{sw}$ values till the youngest part of the record at 1.2 ka (0.07‰ per kyr; $r^2 = 0.5$, $p < 0.01$). The inflection point between these trends at 8–7 ka was found to be statistically significant (probability ~60%). Although large uncertainty exists in this record due to sample resolution as well as age control, we consider the possibility that this trend from ~7 ka toward the present is a signal rather than an artifact.

How can we reconcile opposing Holocene trends in northwestern and northeastern GoM salinity? The lack of secular trends in the Florida Straits' record reinforces the idea that multi-millennial $\delta^{18}O_{sw}$ trends in the northern GoM were not driven by ocean circulation (including the Loop Current and its eddies), which would have impacted the entirety of the Gulf. Moreover, the contrasting zonal $\delta^{18}O_{sw}$ trends refute the idea that monotonic changes in the salinity of Caribbean water masses drove GoM-wide SSS fluctuations (Haug et al., 2001; Poore et al., 2003). Although Poore et al. (2004) suggested that changes in the Intertropical Convergence Zone (ITCZ) position over the Caribbean Sea and its intensity directly impacted salinity downstream in the GoM, our results instead suggest more complex spatial linkages. Alternatively, we propose that disparate North American freshwater influxes and their impact on the mean salinity field in the northern GoM imposed long-term trends in $\delta^{18}O_{sw}$. Though the Orca and Pigmy basins are more proximal to Mississippi-Atchafalaya outflow than the Garrison Basin, all these records together suggest lowered northwestern GoM salinity in the early Holocene. Thus, we hypothesize that the low-salinity plume caused by Mississippi-Atchafalaya runoff during this period extended anomalously westward (c.f., Figure 1), perhaps supplemented by increased outflow from the Rio Grande as well. In addition, heightened mean-annual SSS inferred from the DeSoto Canyon record during the early Holocene indicates that this plume not only extended more westward, but also that its eastern boundary was displaced to the west as well. In this

scenario, the decreasing $\delta^{18}O_{sw}$ trend over the Holocene in the DeSoto Canyon record is explained by the gradual eastward migration of the low-salinity plume toward its modern position, coeval with diminished, westward-flowing freshwater export.

Differing seasonal controls on freshwater export could also bring about contrasting responses in northern GoM salinity over the Holocene. It is well-known that wind-driven, seasonally reversing export pathways exist for Mississippi-Atchafalaya outflow (Morey et al., 2003; Schiller & Kourafalou, 2014). Under modern climatological conditions, peak freshwater discharge during late Boreal Spring is advected eastward (through Ekman transport) in the northern GoM due to southeasterly winds. The opposite occurs during winter, when offshore northerlies transport low-salinity waters associated with late autumnal outflow into the northwestern GoM (Morey et al., 2003). Thus, we hypothesize that orbitally induced changes in insolation could affect seasonal precipitation and runoff, which eventually rectify mean-annual SSS differently across the northern GoM. Additionally, contributions from the Apalachicola and Mobile rivers could have impacted DeSoto Canyon $\delta^{18}O_{sw}$ evolution over the Holocene and similarly, changes in Rio Grande discharge could have also influenced northwestern GoM $\delta^{18}O_{sw}$, independent of the Mississippi-Atchafalaya discharge. These river systems have distinct seasonal expressions of runoff (Dettinger & Diaz, 2000) and thus, future work connecting orbitally induced changes in the seasonal variability of North American river drainage might help attribute the observed trends in $\delta^{18}O_{sw}$ over the Holocene. Finally, we caveat that the trend in the DeSoto Canyon record might arise as an artifact of uncertainty and suggest that a higher-resolution paired record will help clarify the response of northeastern GoM salinity to orbital forcing over the Holocene.

3.4. Comparisons With Reconstructions of Planktic Foraminiferal Populations

We find excellent correspondences between the geochemical reconstructions and planktic foraminiferal assemblages from the interior GoM. We compiled planktic foraminiferal species abundance records from the western (Poore et al., 2003: RC12-10) and northwestern GoM (Poore et al., 2003: Gyre97-6; Poore et al., 2005: MD02-2553) and compared them with the Garrison Basin composite SST and $\delta^{18}O_{sw}$ records. Our intent is to compare broad, millennial-scale changes among the records rather than focus on sub-millennial, high-frequency signals within each record, which has been discussed previously (Poore et al., 2003). To investigate combined variance across all planktic foraminiferal taxa among the records, we computed the first (PC-1) and second principal components (PC-2) at each core site. We found that the PCs across the western GoM characteristically mirrored trends in the Garrison Basin composite records (Figure 7). We grouped PC-1 at RC12-10 (maroon line in Figure 7e; explaining 45% variance) and MD02-2553 (yellow line in Figure 7e; explaining 30% variance) with PC-2 at Gyre97-6 (green line in Figure 7e; explaining 21% variance) as all three records exhibit similar millennial-scale oscillations and trends observed in the Garrison Basin SST composite (Figure 7a). On the other hand, PC-2 from the RC12-10 (maroon line in Figure 7f; explaining 12% variance) and the MD02-2553 (yellow line in Figure 7f; explaining 22% variance) records are strikingly similar to PC-1 from the Gyre97-6 record (green line in Figure 7f; explaining 48% variance), all three of which contain a secular trend coinciding with the multi-millennial salinification trend of the Garrison Basin composite $\delta^{18}O_{sw}$ record (Figure 7b). It is interesting to note that Gyre97-6 is located more closely to the high-salinity conditions of the central GoM compared to the other two core sites containing foraminiferal abundance records (Figure 1). As such, the first leading mode of variability in the Gyre97-6 record exhibits stronger covariance with $\delta^{18}O_{sw}$ ($r^2 = 0.6$, $p < 0.01$) rather than SST changes reconstructed from the Garrison Basin (not significant). Conversely, the second leading mode of variability in the records at the other two sites ($r^2_{RC12\text{-}10} = 0.4$ and $r^2_{MD02\text{-}2553} = 0.3$; $p < 0.01$) were more closely associated with $\delta^{18}O_{sw}$ (Figure 7f). Overall, PCA indicates that planktic foraminiferal ecosystems were intricately coupled to temperature and salinity change in the GoM over the Holocene.

Population abundances of key species driving the leading modes of variability across assemblages also contain strong similarities with the geochemical reconstructions. For example, the abundance of *Orbulina universa*, a mixed-layer dwelling planktic foraminifera shows remarkable replication among the different locations and also exhibits a large millennial-scale variability, with similar relative amplitudes and timing coincident with the early Holocene swings in the Garrison Basin SST record (Figure 7c). Moreover,

millennial-scale variability in *O. universa* abundance persists into the late Holocene and also follows the SST record. Although more work is required to establish causality, one viable explanation for the observed linkage might be that changes in SST also signify changes in the mixed-layer depth and hence, oligotrophic conditions, which, in turn impact *O. universa* populations. In parallel, the relative abundance of *Trilobatus sacculifer*, another mixed-layer dweller (formerly placed in the genus *Globigerinoides*) with an affinity for low-salinity waters in the GoM (Brunner, 1979; Poore et al., 2003), mirrors the long-term increase in $\delta^{18}O_{sw}$ observed in the northwestern GoM records (Figure 7d). Peaking a little later than the $\delta^{18}O_{sw}$ record, *T. sacculifer* populations peak at abundances of ≥25% from 7–6 ka and subsequently diminish to ~5% in the latest Holocene. The trends and patterns of foraminiferal population abundances from three different locations (with different age models) in the western GoM support our interpretation of the geochemical records from the northwestern GoM. Altogether, the planktic foraminiferal assemblages indicate a consistent evolution of surface-ocean conditions alongside the geochemical records.

4. Conclusions

In this work, we have presented sub-centennially resolved proxy composites of surface-ocean temperature and $\delta^{18}O_{sw}$ variability developed from Garrison Basin sediments, northwestern GoM, over the past 11.7 ka. Toward this, we have used paired Mg/Ca and $\delta^{18}O$ measurements in planktic foraminiferal species *G. ruber*, which have been demonstrated to accurately reflect mean annual sea-surface conditions in the GoM. Both SST and $\delta^{18}O_{sw}$ composites exhibit significant centennial-scale variability, but show unique trajectories over the Holocene. The $\delta^{18}O_{sw}$ composite exhibits muted variance in the millennial band and instead contains a secular trend toward higher values (i.e.,higher salinity) from ~8 ka to the present, whereas the long-term SST record contains persistent centennial and millennial-scale fluctuations throughout the Holocene. Previous, albeit shorter records of Holocene climate variability (also developed from foraminiferal geochemistry) in the northwestern GoM align well with our new composite record.

Together with the existing records from the Florida Straits and the northeastern GoM, we uncover strong regional heterogeneity in SST and $\delta^{18}O_{sw}$ evolution over the Holocene. The large millennial-scale SST swings in the early Holocene were only found in the northwestern GoM records, although additional reconstructions of foraminiferal populations from the region support that these features are robust. We hypothesize that changes in the Loop Current and associated implications for its eddy-shedding properties are responsible for millennial-scale SST fluctuations observed in the northwestern GoM. Whereas statistically significant long-term trends in the SST records do not exist, secular trends were found in the northern GoM $\delta^{18}O_{sw}$ records as well as in the foraminiferal assemblage data sets, which are posited to be linked to freshwater outflow from the Mississippi-Atchafalaya and Rio Grande drainage systems. Curiously, we found divergent trends of $\delta^{18}O_{sw}$ in the northeastern and northwestern GoM since the mid-Holocene, which we surmise could be linked to the orbital forcing of different seasons. Accordingly, we recommend caution in causally invoking surface-ocean conditions in the GoM to explain terrestrial paleoclimate changes in one region versus another, wherein careful attention ought to be given to the timescale of variability and region of drainage. Our study demonstrates that the GoM is not one monolithic entity with spatially uniform changes over the Holocene. Instead, Holocene paleoceanography in the GoM was regionally dynamic and variable.

Data Availability Statement

All foraminiferal Mg/Ca and $\delta^{18}O$ data along with the radiocarbon-based age model from this work are archived at the following USGS data release entries: Thirumalai, K., Richey, J.N., Quinn, T.M., and Reynolds, C.E., 2021, Holocene sea-surface temperature and salinity in the Gulf of Mexico: U.S. Geological Survey data release, https://doi.org/10.5066/P9Q5L9VU. Other data sets used in this study are previously published and are archived in repositories according to Lund and Curry (2006), Schmidt and Lynch-Stieglitz (2011), Schmidt et al. (2012), Nürnberg et al. (2008), LoDico et al. (2006), Richey et al. (2007), Richey et al. (2009), Bond et al. (2001), Steinhilber et al. (2012), Poore et al. (2003), Poore et al. (2004), and Poore et al. (2005).

Acknowledgments
We are thankful to Dr. Richard Poore of the USGS for his efforts and support for this project. We gratefully acknowledge Caitlin Reynolds & Jennifer Flannery from the USGS for their assistance with foraminiferal cleaning and elemental analysis. We thank the crew of the R/V Cape Hatteras and Team Paleo at UT Austin for their help in retrieving the core samples. This work was supported by Grant OCE-0902921 to Terrence M. Quinn from the National Science Foundation, and was funded, in part, by the USGS Climate Research and Development Program. Any use of trade, product or firm names is for descriptive purposes only and does not imply endorsement by the U.S. government. Kaustubh Thirumalai acknowledges the UTIG Ewing-Worzel Fellowship, the JSG Lagoe Micropaleontology Fund, and the University of Arizona Technology and Research Initiative Fund (TRIF). Last but not least, we acknowledge Christopher Maupin for reading and critiquing a previous version of this manuscript, and are grateful to two anonymous reviewers, Associate Editor Matthew Lachniet, and Editor Matthew Huber for their efforts in improving our study.

References

Aharon, P. (2006). Entrainment of meltwaters in hyperpycnal flows during deglaciation superfloods in the Gulf of Mexico. *Earth and Planetary Science Letters*, *241*(1–2), 260–270. https://doi.org/10.1016/j.epsl.2005.10.034

Algarra, I., Eiras-Barca, J., Miguez-Macho, G., Nieto, R., & Gimeno, L. (2019). On the assessment of the moisture transport by the great plains low-level jet. *Earth System Dynamics*, *10*(1), 107–119. https://doi.org/10.5194/esd-10-107-2019

Antonarakou, A., Kontakiotis, G., Mortyn, P. G., Drinia, H., Sprovieri, M., Besiou, E., & Tripsanas, E. K. (2015). Biotic and geochemical (δ^{18}o, δ^{18}c, mg/ca, ba/ca) responses of globigerinoides ruber morphotypes to upper water column variations during the last deglaciation, Gulf of Mexico. *Geochimica et Cosmochimica Acta*, *170*(C), 69–93. https://doi.org/10.1016/j.gca.2015.08.003

Arbuszewski, J. A., deMenocal, P. B., Kaplan, A., & Farmer, E. C. (2010). On the fidelity of shell-derived $\delta^{18}o_{sw}$ estimates. *Earth and Planetary Science Letters*, *300*(3–4), 1–12. https://doi.org/10.1016/j.epsl.2010.10.035

Balmaseda, M. A., Mogensen, K., & Weaver, A. T. (2012). Evaluation of the ECMWF ocean reanalysis system ORAS4. *Quarterly Journal of the Royal Meteorological Society*, *139*(674), 1132–1161. https://doi.org/10.1002/qj.2063

Barker, S., Greaves, M., & Elderfield, H. (2003). A study of cleaning procedures used for foraminiferal mg/ca paleothermometry. *Geochemistry, Geophysics, Geosystems*, *4*(9), 1–20. https://doi.org/10.1029/2003gc000559

Bemis, B. E., Spero, H. J., Bijma, J., & Lea, D. W. (1998). Reevaluation of the oxygen isotopic composition of planktonic foraminifera: Experimental results and revised paleotemperature equations. *Paleoceanography*, *13*(2), 150–160. https://doi.org/10.1029/98pa00070

Blaauw, M., & Christen, J. A. (2011). Flexible paleoclimate age-depth models using an autoregressive gamma process. *Bayesian Analysis*, *6*, 457–474. https://doi.org/10.1214/ba/1339616472

Bond, G., Kromer, B., Beer, J., Muschler, R., Evans, M. N., Showers, W., et al. (2001). Persistent solar influence on north atlantic climate during the holocene. *Science*, *294*(5549), 2130–2136. https://doi.org/10.1126/science.1065680

Broecker, W. S., Kennett, J. P., Flower, B. P., Teller, J. T., Trumbore, S., Bonani, G., & Wolfli, W. (1989). Routing of meltwater from the Laurentide ice sheet during the younger dryas cold episode. *Nature*, *341*(6240), 318–321. https://doi.org/10.1038/341318a0

Brokaw, R. J., Subrahmanyam, B., & Morey, S. L. (2019). Loop current and eddy-driven salinity variability in the Gulf of Mexico. *Geophysical Research Letters*, *46*(11), 5978–5986. https://doi.org/10.1029/2019GL082931

Brunner, C. A. (1979). Distribution of planktonic foraminifera in surface sediments of the Gulf of Mexico. *Micropaleontology*, *25*(3), 325. https://doi.org/10.2307/1485306

Candela, J., Ochoa, J., Sheinbaum, J., López, M., Pérez-Brunius, P., Tenreiro, M., et al. (2019). The flow through the gulf of mexico. *Journal of Physical Oceanography*, *49*(6), 1381–1401. https://doi.org/10.1175/jpo-d-18-0189.1

Carter, A., Clemens, S., Kubota, Y., Holbourn, A., & Martin, A. (2017). Differing oxygen isotopic signals of two Globigerinoides ruber (white) morphotypes in the East China Sea: Implications for paleoenvironmental reconstructions. *Marine Micropaleontology*, *131*, 1–9. https://doi.org/10.1016/j.marmicro.2017.01.001

Dettinger, M. D., & Diaz, H. F. (2000). Global characteristics of stream flow seasonality and variability. *Journal of Hydrometeorology*, *1*(4), 289–310. https://doi.org/10.1175/1525-7541(2000)001<0289:gcosfs>2.0.co;2

Dueñas-Bohórquez, A., da Rocha, R. E., Kuroyanagi, A., de Nooijer, L. J., Bijma, J., & Reichart, G.-J. (2011). Interindividual variability and ontogenetic effects on Mg and Sr incorporation in the planktonic foraminifer Globigerinoides sacculifer. *Geochimica et Cosmochimica Acta*, *75*(2), 520–532. https://doi.org/10.1016/j.gca.2010.10.006

Flower, B. P., & Kennett, J. P. (1990). The younger dryas cool episode in the Gulf of Mexico. *Paleoceanography*, *5*(6), 949–961. https://doi.org/10.1029/pa005i006p00949

Gray, W. R., & Evans, D. (2019). Nonthermal influences on Mg/Ca in planktonic foraminifera: A review of culture studies and application to the last glacial maximum. *Paleoceanography and Paleoclimatology*, *34*(3), 306–315. https://doi.org/10.1029/2018pa003517

Gray, W. R., Weldeab, S., Lea, D. W., Rosenthal, Y., Gruber, N., Donner, B., & Fischer, G. (2018). The effects of temperature, salinity, and the carbonate system on Mg/Ca in Globigerinoides ruber (white): A global sediment trap calibration. *Earth and Planetary Science Letters*, *482*, 607–620. https://doi.org/10.1016/j.epsl.2017.11.026

Haug, G. H., Hughen, K. A., Sigman, D. M., Peterson, L. C., & Röhl, U. (2001). Southward migration of the intertropical convergence zone through the holocene. *Science*, *293*(5533), 1304–1308. https://doi.org/10.1126/science.1059725

Hertzberg, J. E., & Schmidt, M. W. (2013). Refining Globigerinoides ruber Mg/Ca paleothermometry in the atlantic ocean. *Earth and Planetary Science Letters*, *383*(C), 123–133. https://doi.org/10.1016/j.epsl.2013.09.044

Holland, K., Branson, O., Haynes, L. L., Hönisch, B., Allen, K. A., Russell, A. D., et al. (2020). Constraining multiple controls on planktic foraminifera Mg/Ca. *Geochimica et Cosmochimica Acta*, *273*, 116–136. https://doi.org/10.1016/j.gca.2020.01.015

Hönisch, B., Allen, K. A., Lea, D. W., Spero, H. J., Eggins, S. M., Arbuszewski, J. A., et al. (2013). The influence of salinity on Mg/Ca in planktic foraminifers – Evidence from cultures, core-top sediments and complementary ? 18o. *Geochimica et Cosmochimica Acta*, *121*, 196–213. https://doi.org/10.1016/j.gca.2013.07.028

Kennett, J. P., & Huddlestun, P. (1972). Late pleistocene paleoclimatology, foraminiferal biostratigraphy and tephrochronology, western Gulf of Mexico. *Quaternary Research 2*(1), 38–69. https://doi.org/10.1016/0033-5894(72)90004-x

Khider, D., Huerta, G., Jackson, C., Stott, L. D., & Emile-Geay, J. (2015). A bayesian, multivariate calibration for Globigerinoides ruber Mg/Ca. *Geochemistry, Geophysics, Geosystems*, *16*, 1–17. https://doi.org/10.1002/2015gc005844

Kısakürek, B., Eisenhauer, A., Böhm, F., Garbe-Schönberg, D., & Erez, J. (2008). Controls on shell Mg/Ca and Sr/Ca in cultured planktonic foraminiferan, Globigerinoides ruber (white). *Earth and Planetary Science Letters*, *273*(3–4), 260–269.

Lambeck, K., Rouby, H., Purcell, A., Sun, Y., & Sambridge, M. (2014). Sea level and global ice volumes from the last glacial maximum to the holocene. *Proceedings of the National Academy of Sciences*, *111*(43), 15296–15303. https://doi.org/10.1073/pnas.1411762111

Lea, D. W., Mashiotta, T. A., & Spero, H. J. (1999). Controls on magnesium and strontium uptake in planktonic foraminifera determined by live culturing. *Geochimica et Cosmochimica Acta*, *63*(16), 2369–2379. https://doi.org/10.1016/s0016-7037(99)00197-0

LeGrande, A. N., & Schmidt, G. A. (2006). Global gridded data set of the oxygen isotopic composition in seawater. *Geophysical Research Letters*, *33*(12), L12604. https://doi.org/10.1029/2006gl026011

Leipper, D. F., & Volgenau, D. (1972). Hurricane heat potential of the Gulf of Mexico. *Journal of Physical Oceanography*, *2*(3), 218–224. https://doi.org/10.1175/1520-0485(1972)002<0218:hhpotg>2.0.co;2

Leventer, A., Williams, D. F., & Kennett, J. P. (1982). Dynamics of the Laurentide ice sheet during the last deglaciation: Evidence from the Gulf of Mexico. *Earth and Planetary Science Letters*, *59*(1), 11–17. https://doi.org/10.1016/0012-821x(82)90112-1

Lin, Y., Greatbatch, R. J., & Sheng, J. (2010). The influence of Gulf of Mexico loop current intrusion on the transport of the Florida current. *Ocean Dynamics*, *60*(5), 1075–1084. https://doi.org/10.1007/s10236-010-0308-0

Liu, Y., Lee, S.-k., Muhling, B. A., Lamkin, J. T., & Enfield, D. B. (2012). Significant reduction of the loop current in the 21st century and its impact on the Gulf of Mexico. *Journal of Geophysical Research*, *117*(C5), C05039. https://doi.org/10.1029/2011jc007555

LoDico, J. M., Flower, B. P., & Quinn, T. M. (2006). Subcentennial-scale climatic and hydrologic variability in the Gulf of Mexico during the early holocene. *Paleoceanography*, *21*(3), PA3015. https://doi.org/10.1029/2005pa001243

Lund, D. C., & Curry, W. B. (2006). Florida current surface temperature and salinity variability during the last millennium. *Paleoceanography*, *21*(2), PA2009. https://doi.org/10.1029/2005pa001218

Mathien-Blard, E., & Bassinot, F. (2009). Salinity bias on the foraminifera Mg/Ca thermometry: Correction procedure and implications for past ocean hydrographic reconstructions. *Geochemistry, Geophysics, Geosystems*, *10*(12), 1–17. https://doi.org/10.1029/2008gc002353

Metcalfe, S. E., Barron, J. A., & Davies, S. J. (2015). The holocene history of the north american monsoon: 'known knowns' and 'known unknowns' in understanding its spatial and temporal complexity. *Quaternary Science Reviews*, *120*(C), 1–27. https://doi.org/10.1016/j.quascirev.2015.04.004

Misra, V., Li, H., & Kozar, M. (2014). The precursors in the Intra-Americas seas to seasonal climate variations over North America. *Journal of Geophysical Research: Oceans*, *119*(5), 2938–2948. https://doi.org/10.1002/2014jc009911

Montero-Serrano, J. C., Bout-Roumazeilles, V., Sionneau, T., Tribovillard, N., Bory, A., Flower, B. P., et al. (2010). Changes in precipitation regimes over North America during the holocene as recorded by mineralogy and geochemistry of Gulf of Mexico sediments. *Global and Planetary Change*, *74*(3–4), 132–143. https://doi.org/10.1016/j.gloplacha.2010.09.004

Morey, S. L., Martin, P. J., O'Brien, J. J., Wallcraft, A. A., & Zavala-Hidalgo, J. (2003). Export pathways for river discharged fresh water in the northern Gulf of Mexico. *Journal of Geophysical Research: Oceans*, *108*(C10). https://doi.org/10.1029/2002jc001674

Nürnberg, D., Bijma, J., & Hemleben, C. (1996). Assessing the reliability of magnesium in foraminiferal calcite as a proxy for water mass temperatures. *Geochimica et Cosmochimica Acta*, *60*(5), 803–814. https://doi.org/10.1016/0016-7037(95)00446-7

Nürnberg, D., Ziegler, M., Karas, C., Tiedemann, R., & Schmidt, M. W. (2008). Interacting loop current variability and Mississippi river discharge over the past 400 kyr. *Earth and Planetary Science Letters*, *272*(1–2), 278–289. https://doi.org/10.1016/j.epsl.2008.04.051

Pilcher, R. S., & Blumstein, R. D. (2007). Brine volume and salt dissolution rates in orca basin, northeast Gulf of Mexico. *AAPG Bulletin*, *91*(6), 823–833. https://doi.org/10.1306/12180606049

Poore, R. Z., Dowsett, H. J., Verardo, S., & Quinn, T. M. (2003). Millennial- to century-scale variability in Gulf of Mexico holocene climate records. *Paleoceanography*, *18*(2), 1048. https://doi.org/10.1029/2002pa000868

Poore, R. Z., Pavich, M. J., & Grissino-Mayer, H. D. (2005). Record of the North American southwest monsoon from Gulf of Mexico sediment cores. *Geology*, *33*(3), 209–204. https://doi.org/10.1130/g21040.1

Poore, R. Z., Quinn, T. M., & Verardo, S. (2004). Century-scale movement of the Atlantic intertropical convergence zone linked to solar variability. *Geophysical Research Letters*, *31*(12), L12214. https://doi.org/10.1029/2004gl019940

Rayner, N. A., Parker, D. E., Horton, E. B., Folland, C. K., Alexander, L. V., Rowell, D. P., et al. (2003). Global analyses of sea surface temperature, sea ice, and night marine air temperature since the late nineteenth century. *Journal of Geophysical Research*, *108*(D14), 4407–4437. https://doi.org/10.1029/2002jd002670

Reimer, P. J., Bard, E., Bayliss, A., Beck, W. J., Blackwell, P. G., Ramsey, C. B., et al. (2013). IntCal13 and Marine13 radiocarbon age calibration curves 0-50,000 years cal BP. *Radiocarbon*, *55*(4), 1869–1887. https://doi.org/10.2458/azu_js_rc.55.16947

Richey, J. N., Poore, R. Z., Flower, B. P., & Quinn, T. M. (2007). 1400 yr multiproxy record of climate variability from the northern Gulf of Mexico. *Geology*, *35*(5), 423–424. https://doi.org/10.1130/g23507a.1

Richey, J. N., Poore, R. Z., Flower, B. P., Quinn, T. M., & Hollander, D. J. (2009). Regionally coherent Little Ice Age cooling in the Atlantic Warm Pool. *Geophysical Research Letters*, *36*(21), L21703. https://doi.org/10.1029/2009gl040445

Richey, J. N., Thirumalai, K., Khider, D., Reynolds, C. E., Partin, J. W., & Quinn, T. M. (2019). Considerations for Globigerinoides ruber (white and pink) paleoceanography: Comprehensive insights from a long-running sediment trap. *Paleoceanography and Paleoclimatology*, *313*(5785), 345–347.

Ruggieri, E. (2012). A bayesian approach to detecting change points in climatic records. *International Journal of Climatology*, *33*(2), 520–528. https://doi.org/10.1002/joc.3447

Sackett, W. M., & Rankin, J. G. (1970). Paleotemperatures for the Gulf of Mexico. *Journal of Geophysical Research*, *75*(24), 4557–4560. https://doi.org/10.1029/jc075i024p04557

Sadekov, A., Eggins, S. M., De Deckker, P., Ninnemann, U., Kuhnt, W., & Bassinot, F. (2009). Surface and subsurface seawater temperature reconstruction using Mg/Ca microanalysis of planktonic foraminifera *Globigerinoides ruber, Globigerinoides sacculifer, and Pulleniatina obliquiloculata*. *Paleoceanography*, *24*(3), 1–17. https://doi.org/10.1029/2008pa001664

Saenger, C. P., & Evans, M. N. (2019). Calibration and validation of environmental controls on planktic foraminifera Mg/Ca using global core-top data. *Paleoceanography and Paleoclimatology*, *34*(8), 1249–1270. https://doi.org/10.1029/2018pa003507

Schiller, R., & Kourafalou, V. (2014). Loop current impact on the transport of mississippi river waters. *Journal of Coastal Research*, *298*, 1287–1306. https://doi.org/10.2112/jcoastres-d-13-00025.1

Schmidt, M. W., & Lynch-Stieglitz, J. (2011). Florida Straits deglacial temperature and salinity change: Implications for tropical hydrologic cycle variability during the Younger Dryas. *Paleoceanography*, *26*(4). PA4205. https://doi.org/10.1029/2011pa002157

Schmidt, M. W., Weinlein, W. A., Marcantonio, F., & Lynch-Stieglitz, J. (2012). Solar forcing of Florida Straits surface salinity during the early holocene. *Paleoceanography*, *27*(3), PA3204. https://doi.org/10.1029/2012pa002284

Schrag, D. P. (1999). Rapid analysis of high-precision Sr/Ca ratios in corals and other marine carbonates. *Paleoceanography*, *14*(2), 97–102. https://doi.org/10.1029/1998pa900025

Steinhilber, F., Abreu, J. A., Beer, J., Brunner, I., Christl, M., Fischer, H., et al. (2012). 9,400 years of cosmic radiation and solar activity from ice cores and tree rings. *Proceedings of the National Academy of Sciences*, *109*(16), 5967–5971. https://doi.org/10.1073/pnas.1118965109

Steinke, S., Chiu, H.-Y., Yu, P.-S., Shen, C.-C., Löwemark, L., Mii, H.-S., & Chen, M.-T. (2005). Mg/Ca ratios of two Globigerinoides ruber (white) morphotypes: Implications for reconstructing past tropical/subtropical surface water conditions. *Geochemistry, Geophysics, Geosystems*, *6*(11), Q11005. https://doi.org/10.1029/2005gc000926

Sturges, W., & Leben, R. (2000). Frequency of ring separations from the loop current in the Gulf of Mexico: A revised estimate. *Journal of Physical Oceanography*, *30*(7), 1814–1819. https://doi.org/10.1175/1520-0485(2000)030<1814:forsft>2.0.co;2

Thirumalai, K., Quinn, T. M., & Marino, G. (2016). Constraining past seawater δ^{18}o and temperature records developed from foraminiferal geochemistry. *Paleoceanography*, *31*(10), 1409–1422. https://doi.org/10.1002/2016PA002970

Thirumalai, K., Quinn, T. M., Okumura, Y., Richey, J. N., Partin, J. W., Poore, R. Z., & Moreno-Chamarro, E. (2018). Pronounced centennial-scale Atlantic ocean climate variability correlated with western hemisphere hydroclimate. *Nature Communications*, *9*(1), 113–111. https://doi.org/10.1038/s41467-018-02846-4

Thirumalai, K., Richey, J. N., Quinn, T. M., & Poore, R. Z. (2014). Globigerinoides ruber morphotypes in the Gulf of Mexico: A test of null hypothesis. *Scientific Reports*, *4*, 1–7. https://doi.org/10.1038/srep06018

Thirumalai, K., Singh, A., Ramesh, R., & Ramesh, R. (2011). A MATLAB™ code to perform weighted linear regression with (correlated or uncorrelated) errors in bivariate data. *Journal of the Geological Society of India*, *77*(4), 377–380. https://doi.org/10.1007/s12594-011-0044-1

Tierney, J. E., Malevich, S. B., Gray, W., Vetter, L., & Thirumalai, K. (2019). Bayesian calibration of the Mg/Ca paleothermometer in planktic foraminifera. *Paleoceanography and Paleoclimatology*, *34*(12), 2005–2030. https://doi.org/10.1029/2019pa003744

Tierney, J. E., Pausata, F. S. R., & deMenocal, P. B. (2015). Deglacial indian monsoon failure and North Atlantic Stadials linked by Indian Ocean surface cooling. *Nature Geoscience*, *9*, 46–50. https://doi.org/10.1038/ngeo2603

Vetter, L., Spero, H. J., Eggins, S. M., Williams, C., & Flower, B. P. (2017). Oxygen isotope geochemistry of Laurentide ice-sheet meltwater across Termination I. *Quaternary Science Reviews*, *178*, 102–117. https://doi.org/10.1016/j.quascirev.2017.10.007

Wagner, A. J., Guilderson, T. P., Slowey, N. C., & Cole, J. E. (2009). Pre-bomb surface water radiocarbon of the Gulf of Mexico and Caribbean as recorded in Hermatypic corals. *Radiocarbon*, *51*(3), 947–954. https://doi.org/10.1017/s0033822200034020

Wagner, A. J., & Slowey, N. C. (2011). Oxygen isotopes in seawater from the Texas-Louisiana shelf. *Bulletin of Marine Science*, *87*(1), 1–12. https://doi.org/10.5343/bms.2010.1004

Wang, C., & Enfield, D. B. (2003). A further study of the tropical western hemisphere warm pool. *Journal of Climate*, *16*(10), 1476–1493. https://doi.org/10.1175/1520-0442-16.10.1476

Wang, L. (2000). Isotopic signals in two morphotypes of Globigerinoides ruber (white) from the South China Sea: Implications for monsoon climate change during the last glacial cycle, *Palaeogeography, Palaeoclimatology. Palaeoecology*, *161*(3–4), 381–394. https://doi.org/10.1016/s0031-0182(00)00094-8

Wanner, H., Mercolli, L., Grosjean, M., & Ritz, S. P. (2015). Holocene climate variability and change; a data-based review. *Journal of the Geological Society*, *172*(2), 254–263. https://doi.org/10.1144/jgs2013-101

Wanner, H., Solomina, O. N., Grosjean, M., Ritz, S. P., & Jetel, M. (2011). Structure and origin of holocene cold events. *Quaternary Science Reviews*, *30*, 1–15. https://doi.org/10.1016/j.quascirev.2011.07.010

Williams, C., Flower, B. P., & Hastings, D. W. (2012). Seasonal Laurentide ice sheet melting during the "mystery interval" (17.5–14.5 ka). *Geology*, *40*(10), 955–958. https://doi.org/10.1130/g33279.1

Zhang, L., Wang, C., & Lee, S.-k. (2014). Potential role of Atlantic warm pool-induced freshwater forcing in the Atlantic meridional overturning circulation: Ocean–sea ice model simulations. *Climate Dynamics*, *43*(1–2), 553–574. https://doi.org/10.1007/s00382-013-2034-z